Common Mode Voltage Reduction Schemes for Voltage Source Converters in an Autonomous Microgrid

Tazay Ahmad, *Student Member, IEEE,* and Zhixin Miao, *Senior Member, IEEE*

***Abstract*—Voltage-sourced converter (VSC) is becoming the key element in the operation of microgrids due to its high performance and efficiency. However, implementing VSC may generate some issues to the microgrid such as high common mode voltage (CMV). CMV could produce high leakage current and bearing failure in case of motor load.**

This paper develops a solution for high CMV using reduced CMV-PWM algorithm to control of VSC with interfaced source in an autonomous microgrid. It also investigates the performance of V/F controller of VSC when reduced CMV-PWM technique is applied. The following approaches are implemented to provide detailed procedures for reducing CMV of VSC. First, a microgrid with V/F vector control is illustrated. Second, a reduced CMV-PWM method is investigated and compared with conventional PWM technique. Finally, a microgrid is modeled and simulated in PSCAD/EMTDC to validate reduced CMV-PWM technique.

***Index Terms*—Microgrid, Vector Control, Voltage-Sourced Converter (VSC), Common-mode Voltage (CMV), SVPWM, AZPWM.**

I. Introduction

Power electronics play an important role in converting DC power into AC power from distributed generators (DGs) to controllable loads. IGBT based voltage-sourced converter (VSC) is one of the commonly used power electronic devices that are recently implemented in controlling a microgrid due to several advantages. The benefits of using VSC include independent control of voltage and frequency, possibility to be connected to a weak ac grid and ability to mitigate the negative effect of disturbance [1]–[3].

Several pulse width modulation (PWM) methods have been developed to control the switching pulses of VSC [4]. Sinusoidal pulse width modulation (SPWM) and space vector pulse width modulation (SVPWM) are commonly used methods to control of switching state patterns of VSC. The advantages of implementing SPWM and SVPWM include good AC and DC current ripple, low switching frequency and high voltage linearity range [5]. However, they generate high common mode voltage (CMV) which may produce some problems to the system. These issues cause a failure in the stator winding insulations, bearing currents and high frequency leakage current on the motors as well as affect the operation of circuit breakers of the loads [6].

Common mode voltage (CMV) is defined as the potential difference voltage between star point of the load and the center of the $C_{\mathrm{dc-link}}$ of the DC bus. The general schematic diagram of three-phase two-level VSC based microgrid is shown in Fig. 1. The CMV for three-phase two-level VSC is given in the following equation:

$$V_{com} = \frac{V_{ao} + V_{bo} + V_{co}}{3} \quad (1)$$

Generally, CMV equals zero when the load receives balanced three-phase sinusoidal phase voltages. Since VSC generates high current harmonics, high CMV is produced on the load's terminal.

Several approaches have been recently investigated to mitigate and eliminate CMV [7], [8]. The authors proposed hardware devices to eliminate CMV. However, using hardware elements and filters require additional complexity and cost to the system which are not a recommended solution ofr economical perspective. Beside, applying software method is an effective solution to reduce common mode voltage (RCMV) at no cost.

This paper provides a technique for reducing CMV-PWM for three-phase two-level VSC based microgrid at autonomous mode. It also investigates the advantages of implementing RCMV-PWM comparing with conventional PWM algorithm. In addition, designing V/F vector control of VSC is presented in this paper.

The rest of the paper is organized as follows. Section II describes the system design and control concept of VSC based autonomous microgrid. It also develops mathematical model and tuning techniques of the transfer function equations. Section III provides a technique to reduce CMV. Section IV tests the performance of the designing controller by applying several case studies. The examination of the performance of the system is simulated by PSCAD/EMTDC software.

II. System Design and Control Concept

Vector control methodology is used to control the voltage and frequency of VSC [9], [10]. A general scheme of transformerless VSC at an autonomous microgrid is shown in Fig. 1. The concept of vector control depends on transferring symmetrical signals from three-phase time domain into two-phase rotating synchronous reference frame.

Fig. 2 shows a phase circuit diagram of VSC based microgrid at autonomous mode. The dynamic equations of the system in Fig. 2 are analyzed to find the states and controlled variables of the system. Two main components need to be controlled which are output current and voltage of VSC. The

Z. Miao, and A. Tazay are with the Department of Electrical Engineering, University of South Florida, Tampa, FL 33620 USA (e-mail: zmiao@usf.edu; ahmadtazay@mail.usf.edu).

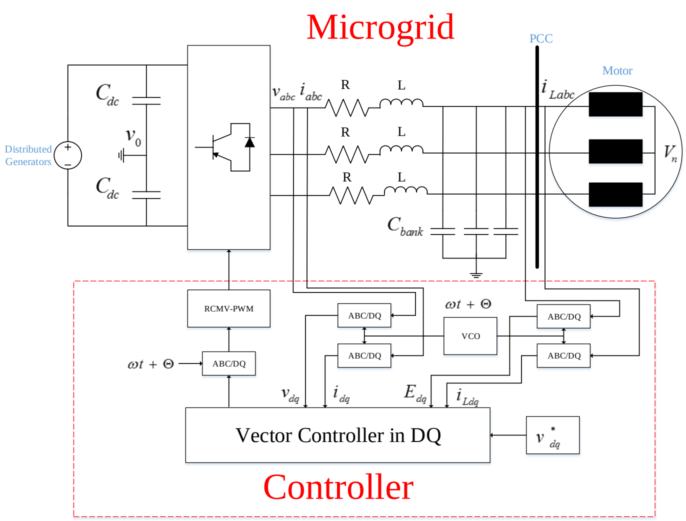

Fig. 1. General scheme of a VSC using vector control.

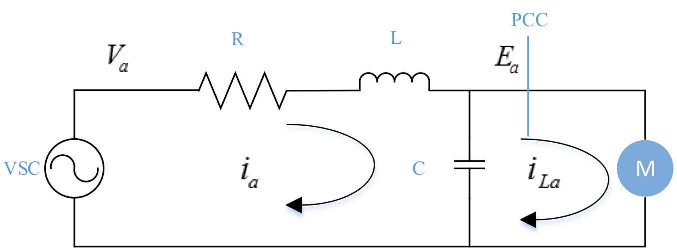

Fig. 2. Phase circuit diagram of an autonomous microgrid.

dynamic equations of the inner current loop and outer voltage loop are given as follows:

$$L\frac{di_{\text{abc}}}{dt} = -Ri_{\text{abc}} + V_{\text{abc}} - E_{\text{abc}} \tag{2}$$

$$C\frac{dV_{C_{\text{abc}}}}{dt} = i_{\text{abc}} - i_{\text{labc}} \tag{3}$$

The current and voltage equations in (2) and (3) are then transferred into DQ reference frame as follows:

$$C\frac{dV_{sd}}{dt} = C\omega V_{sq} + i_d - i_{ld} \tag{4}$$

$$C\frac{dV_{sq}}{dt} = -C\omega V_{sd} + i_q - i_{lq} \tag{5}$$

$$L\frac{di_d}{dt} = -Ri_d + L\omega(t)i_q + V_{sd} \tag{6}$$

$$L\frac{di_q}{dt} = -Ri_q - L\omega(t)i_d + V_{sq} \tag{7}$$

Designing V/F controller basically depends on determining the optimal operating structure of the system and regulating the compensators. These elements have to accomplish stability, fast response and disturbance rejection. Since all signals are transferred into DQ reference frame, PI controller is a sufficient compensator to provide zero steady state error [11].

The open-loop transfer function of the inner current controller is illustrated as:

$$\begin{aligned} l_i(s) &= K_i(s)P_i(s) \\ &= \left(k_{ip} + \frac{k_{ii}}{s}\right)\frac{1}{Ls+R} \end{aligned} \tag{8}$$

The order of the closed-loop transfer function of the current is less than 3 which is recommended to use "Modulus Optimum" technique [12]. This method is suitable to tune the parameters of the inner current compensator because of its simplicity and accuracy.

The open-loop transfer function of the current is obtained as follows:

$$l_i = K_{ip}\left(\frac{s+\frac{K_{ii}}{K_{ip}}}{s}\right)\frac{1}{L(s+\frac{R}{L})} \tag{9}$$

$$= \frac{K_p}{R\tau_i s} \tag{10}$$

where τ_i is the desired closed-loop time constant. The dominate pole of the plant can be canceled by adjusting the zero of PI-compensator. By letting $K_{ip} = \frac{L}{\tau_i}$ and $K_{ii} = \frac{R}{\tau_i}$, the closed loop response can achieve the designing requirements. The open and closed loop transfer functions of the inner current will be formed as:

$$G_{i_{ol}} = \frac{K_{ip}}{Ls} \tag{11}$$

$$G_{i_{cl}} = \frac{K_{ip}}{Ls+K_{ip}} = \frac{1}{\tau_i s+1} \tag{12}$$

The open loop transfer function of the voltage controller is given as:

$$\begin{aligned} l_v(s) &= K_v(s)G_{icl}(s)P_v(s) \\ &= \left(k_{vp} + \frac{k_{vi}}{s}\right)\left(\frac{1}{\tau_i s+1}\right)\left(\frac{1}{Cs}\right) \end{aligned} \tag{13}$$

The detailed equations for tuning the outer voltage loop are illustrated as follows:

$$\omega_{\text{cutoff}} = \frac{1}{\sqrt{T_v\tau_i}} \tag{14}$$

$$\Phi_{\text{max}} = \sin^{-1}\left(\frac{T_v-\tau_i}{T_s+\tau_i}\right) \tag{15}$$

$$K_{vp} = C\omega_{\text{cutoff}} \tag{16}$$

where ω_{cutoff}, T_v and Φ_{max} are outer-loop cutoff frequency, compensator time constant and maximum open-loop phase margin, respectively. Regulating the load voltage is achieved by controlling of the magnitude of voltage components in DQ reference frame that is presented as $V_s = \sqrt{v_{sd}^2 + v_{sq}^2}$ while the frequency is provided by voltage-controlled oscillator (VCO).

The desire of tuning the inner controller is to achieve fast response. Beside, the main goal of designing the outer loop is optimum regulation and stability. The selected parameters and bandwidth of the designed inner current and outer voltage loops are given in Table I. The overall V/F control algorithm of VSC based autonomous mode is shown in Fig. 3. The figure shows the vector control of the voltages on dq-axis where the frequency is constant and given from VCO.

TABLE I
PARAMETERS OF THE CURRENT AND VOLTAGE CONTROLLERS.

ω_n	377 rad/sec	K_{ip}	4.28 Ω
$\omega_{\text{switching}}$	19000 rad/sec	K_{ii}	2000 Ω/sec
ω_i	2000 rad/sec	K_{vp}	0.6699 Ω^{-1}
ω_v	1000 rad/sec	T_v	4.5 msec
ω_{cutoff}	670 rad/sec	Φ_{max}	53^o

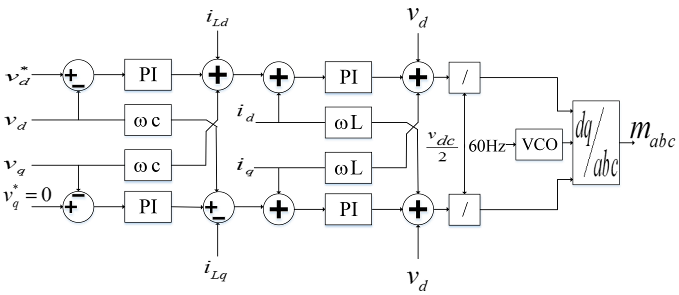

Fig. 3. V/F control algorithm for VSC at autonomous mode.

III. PWM METHODS

A. SVPWM

Two main methods are used to control of switching patterns for VSC. Scalar and space vector techniques provide almost the same equivalent performance in case of practical and theoretical implementations. Scalar method such as SPWM where sinusoidal signals compare with high frequency triangular signal, is more favorable for implementation due to simplicity. Vector algorithm such as SVPWM is preferable due to large utilization voltage linearity and digital implementation [13].

The concept of SVPWM consist of implementation complex voltage vector states to approximate the reference voltage vector in a sampling time period. This technique provides controlling the sequence of switching states. The vector transformation of two-level three phase VSC into $\alpha\beta$ domain contains eight vector states, $2^3 = 8$, which include six active states and two zero states.

The representation of space vector is illustrated as following:

$$\overrightarrow{V_s}(t) = \frac{2}{3}[e^{j0}V_a(t) + e^{j\frac{2}{3}\pi}V_b(t) + e^{j\frac{4}{3}\pi}V_c(t)] \qquad (17)$$

The reference signal has the following definition in space vector domain:

$$\overrightarrow{V_s} = \frac{2}{3}\sqrt{2}|V|e^{j(\omega t+\theta)} \qquad (18)$$

The reference voltage is calculated based on the transformation of V_{abc} into vector signals on rotating reference frame. The magnitude and angle of the reference signal is given as:

$$|\vec{V_s}| = \sqrt{(V_d)^2 + (V_q)^2} \qquad (19)$$

$$\alpha = \tan^{-1}(\frac{V_q}{V_d}) \qquad (20)$$

The space vectors of VSC divides the complex domain into six vectors. The six active vectors ($V_1, V_2, V_3, V_4, V_5, V_6$) and the two zero vectors (V_0, V_7) are fixed in the rotating reference frame during sampling time and divide the complex plan into six sectors. The fundamental signal are rotating at speed of fundamental angular speed ωt with constant magnitude.

The reference vector in SVPWM is synthesized by two active vectors and a zero vector. In order to reduce switching losses, two adjacent active vectors and two zero vectors are adopted to synthesize the reference vector as shown in Fig. 4.a) where the reference vector is located at sector one.

B. Reduce CMV-PWM

The main reason of high CMV is selecting zero state vectors to synthesize the reference signal. SVPWM divides the zero state time between the two zero states to synthesize the reference signal. Zero state vectors actually generate high CMV which reaches up to 50% of V_{dc} while active state vectors produce 17% of V_{dc} [6]. So, avoiding selecting zero save vectors is essential to reduce CMV.

Reduce CMV-PWM implements only active vectors and avoids selecting zero-vectors which are the cause of CMV. The proposed algorithm aims to select only active space vectors to represent the reference signal. Active zero state pulse width modulation (AZPWM) algorithm implements the same concept of SVPWM to synthesize the reference signal. Beside, it selects two opposite active vectors with equal time durations to synthesize the reference signal instead of zero vectors as shown in Fig. 4.b).

The representation of reference vector depends on the notion of volt-seconds balance rule. The reference vector in Fig. 4.b) is synthesized by two adjacent active vectors and two opposite active vectors as shown in Eqn. (21):

$$\overrightarrow{V_s}T_s = \overrightarrow{V_n}T_n + \overrightarrow{V_{n+1}}T_{n+1} + \overrightarrow{V_{n+2}}T_{n+2} + \overrightarrow{V_{n-1}}T_{n-1} \quad (21)$$

where T_n, T_s, and V_n are dwelling times, sampling time and selected vector, respectively.

The performance of AZPWM depends mainly on the voltage utilization level M_i. The magnitude value of the six active vectors, modulation index, and dwelling time of each sector are given the following equations:

$$V_n = \frac{3}{2}|V_{dc}|e^{(n-1)\frac{\pi}{3}} \qquad (22)$$

$$M_i = \frac{|V_{ref}|}{V_{steps}} = \frac{\pi V_{ref}}{2V_{dc}} \qquad (23)$$

$$T_n = \frac{2\sqrt(3)T_sMI}{\pi}\left(\sin(\frac{n\pi}{3})\cos\theta\right) - \left(\cos(\frac{n\pi}{3})\sin\theta\right) \qquad (24)$$

$$T_{n+1} = \frac{2\sqrt(3)T_sMI}{\pi}\left(-\sin(\frac{(n-1)\pi}{3})\cos\theta\right) - \left(\cos(\frac{(n-1)\pi}{3})\sin\theta\right) \qquad (25)$$

$$T_s = T_a + T_b + T_{n-1} + T_{n+2} \qquad (26)$$

$$T_{n+2} = T_{n-1} \qquad (27)$$

One more important segment in reducing switching losses is to determine the switching sequence. In [14], it is claimed

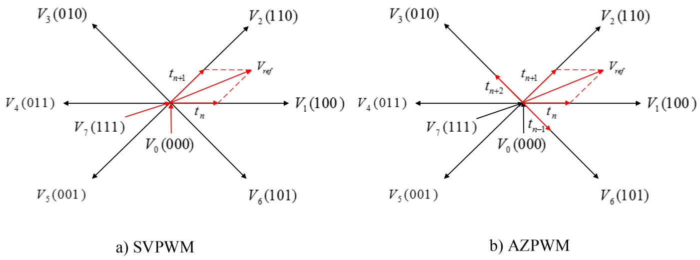

Fig. 4. SVPWM and AZPWM representation at $\alpha\beta$ reference.

that the time sequence of the dwelling time based on 7-segment method has lowest total harmonic distortion. Each switches has to change it's state once at every switching period to achieve optimal harmonic performance and lowest switching frequency. The concept of 7-segment is shown in Fig. 5 for both SVPWM and AZPWM algorithms. Fig. 5 shows the comparison between SVPWM and AZPWM according to CMV. It can be seen from Fig. 5 that CMV can be reduced if only active vectors are selected. The switching

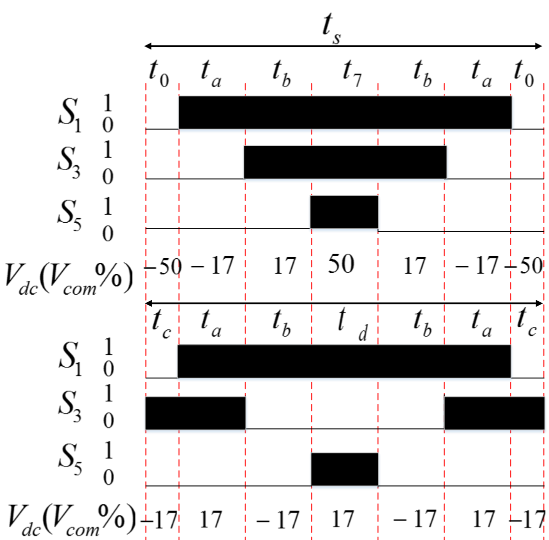

Fig. 5. Switching sequence based on 7-segment method for sector one. Top figure is CMV with switching sequence for SVPWM at sector 1. Bottom figure is CMV with switching sequence for AZPWM at sector 1.

sequences for SVPWM and AZPWM at each sector are given in Table II.

TABLE II
SWITCHING SEQUENCE FOR SVPWM AND AZPWM.

Sector	SVPWM	AZPWM1
1	0127210	3216123
2	0237320	4321234
3	0437340	5432345
4	0457540	6543456
5	0657560	1654561
6	0617160	2165612

IV. SIMULATION RESULTS OF THE SYSTEM

The designing of V/F vector control based on AZPWM of VSC is achieved in PSCAD/EMTDC. The overall scheme of an autonomous microgrid is shown in Fig. 6. In order to validate the method, an induction motor is added at no load. SVPWM and AZPWM algorithm are studied to compare the impact of CMV on the load as well as investigate the robustness of the controller on load's disturbance. The rated parameters of the microgrid are given in Table III.

V/F controller's behavior is shown in Fig. 7. The voltage

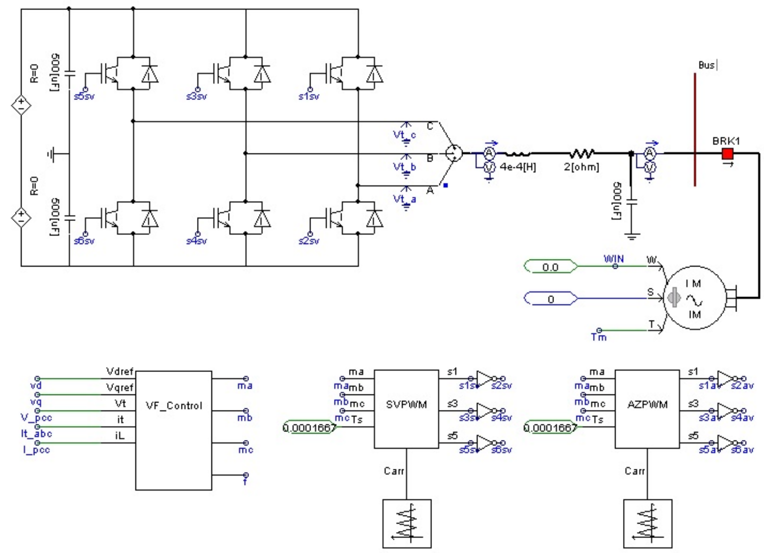

Fig. 6. Schematic diagram of a microgrid at autonomous mode.

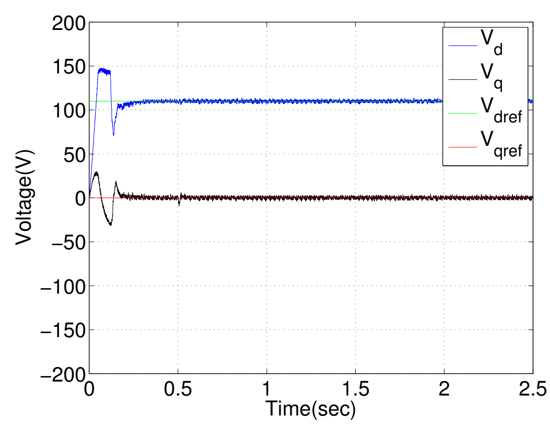

Fig. 7. Voltage of microgrid when V/F controller is used.

V_d sets to equal the nominal voltage while the voltage V_q equals zero. Induction motor is connected at 0.5 second to represent the effect of CMV on the system as well as investigate the capability of the controller. From the figure, it can be observed V/F controller can keep the dq-axis to the reference values which is 110 V.

Two common PWM algorithms are used to investigate the behavior of CMV which are SVPWM and AZPWM. The switching frequency is set at 6 kHz for both methods. The modulation index is kept constant at 0.7 since the voltage is fixed for the microgrid. Figs. 8 and 9 shows the behavior of CMV when SVPWM and AZPWM algorithms are implemented. They also provides phase line current wave and motor's torques and speed. It can be noticed from Figs. 8 and 9 that the AZSPWM algorithms can reduce CMV variations when compared with the SVPWM algorithm. The reduction of CMV can be achieved by 17%.

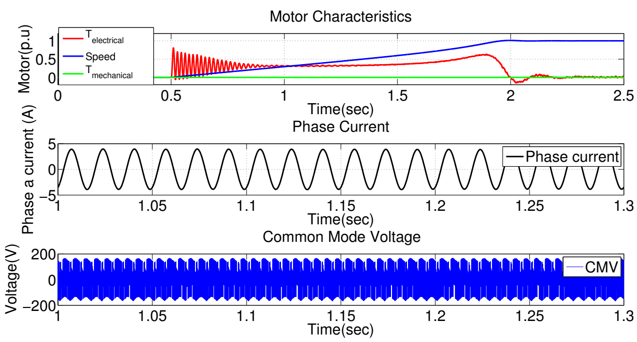

Fig. 8. SVPWM based VSC for autonomous microgrid. Top figure is the torques and speed of the IM. Middle figure is the phase line current. Bottom figure is the CMV.

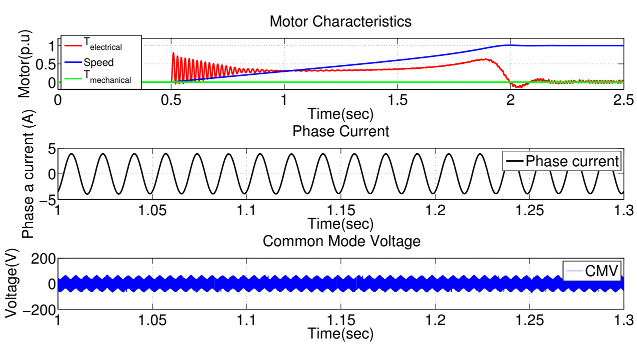

Fig. 9. AZPWM based VSC for autonomous microgrid. Top figure is the torques and speed of the IM. Middle figure is the phase line current. Bottom figure is the CMV.

TABLE III
RATED PARAMETERS OF MICROGRID.

Microgrid Components	Values	AC System	Values
L	40 mH	V_{LL}	$110 \times \sqrt{3}$ V
R	2Ω	$F_{\text{fundamental}}$	60 Hz
V_{dc}	300 V	P_{motor}	4 kW
$C_{\text{dc-link}}$	500 uF	M_{pole}	4
$F_{\text{switching}}$	6 kHz	M_{speed}	1440 min^{-1}

V. CONCLUSION

The consequences of applying reduced CMV-PWM method for VSC based of microgrid at grid-connected mode with induction motor load are presented in this paper. In this paper, implementation of AZPWM based VSC at an autonomous mode is presented. The paper investigates the performance of AZPWM algorithm and compares with standard SVPWM method. VSC is used to control the voltage and frequency in autonomous microgrid. The paper provides a method to reduce CMV for control V/F and switching states of VSC at the terminal induction motor's load. Designing and tuning V/F controller of VSC are also provided. AZPWM shows that CMV has been reduced by 17% of V_{dc} instead of 50% of V_{dc} when SVPWM is applied. It can also be seen that applying AZPWM provides stability to V/F controller in case of any disturbance. The simulation by PSCAD confirmed the effectiveness of reducing CMV using AZPWM method.

ACKNOWLEDGEMENT

The authors would like to thank Dr. Lingling Fan for her valuable comments and suggestions to improve the quality of the paper.

REFERENCES

[1] J. Carrasco, L. Franquelo, J. Bialasiewicz, E. Galvan, R. Guisado, M. Prats, J. Leon, and N. Moreno-Alfonso, "Power-electronic systems for the grid integration of renewable energy sources: A survey," *Industrial Electronics, IEEE Transactions on*, vol. 53, no. 4, pp. 1002–1016, June 2006.

[2] N. Flourentzou, V. Agelidis, and G. Demetriades, "Vsc-based hvdc power transmission systems: An overview," *Power Electronics, IEEE Transactions on*, vol. 24, no. 3, pp. 592–602, March 2009.

[3] R. Lasseter, "Microgrids," in *Power Engineering Society Winter Meeting, 2002. IEEE*, vol. 1, 2002, pp. 305–308 vol.1.

[4] J. Holtz, "Pulsewidth modulation-a survey," *Industrial Electronics, IEEE Transactions on*, vol. 39, no. 5, pp. 410–420, 1992.

[5] H. W. Van Der Broeck, H.-C. Skudelny, and G. V. Stanke, "Analysis and realization of a pulsewidth modulator based on voltage space vectors," *Industry Applications, IEEE Transactions on*, vol. 24, no. 1, pp. 142–150, 1988.

[6] A. M. Hava and E. Un, "Performance analysis of reduced common-mode voltage pwm methods and comparison with standard pwm methods for three-phase voltage-source inverters," *Power Electronics, IEEE Transactions on*, vol. 24, no. 1, pp. 241–252, 2009.

[7] M. Swamy, K. Yamada, and T. Kume, "Common mode current attenuation techniques for use with pwm drives," *Power Electronics, IEEE Transactions on*, vol. 16, no. 2, pp. 248–255, Mar 2001.

[8] G. Skibinski, R. Kerkman, and D. Schlegel, "Emi emissions of modern pwm ac drives," *Industry Applications Magazine, IEEE*, vol. 5, no. 6, pp. 47–80, Nov 1999.

[9] M. Kazmierkowski and L. Malesani, "Current control techniques for three-phase voltage-source pwm converters: a survey," *Industrial Electronics, IEEE Transactions on*, vol. 45, no. 5, pp. 691–703, Oct 1998.

[10] L. Xu, Z. Miao, and L. Fan, "Control of a back-to-back vsc system from grid-connection to islanded mode in microgrids," in *Energytech, 2011 IEEE*. IEEE, 2011, pp. 1–6.

[11] A.Tazay, L. Fan, and Z. Miao., "Black start of an induction motor in an autonomous microgrid," *to appear, IEEE PESGM 2014.*

[12] C. Bajracharya, M. Molinas, J. A. Suul, T. M. Undeland *et al.*, "Understanding of tuning techniques of converter controllers for vsc-hvdc," in *Nordic Workshop on Power and Industrial Electronics (NORPIE/2008), June 9-11, 2008, Espoo, Finland*. Helsinki University of Technology, 2008.

[13] A. M. Hava, R. J. Kerkman, and T. A. Lipo, "Simple analytical and graphical methods for carrier-based pwm-vsi drives," *Power Electronics, IEEE Transactions on*, vol. 14, no. 1, pp. 49–61, 1999.

[14] W.-F. Zhang and Y.-H. Yu, "Comparison of three svpwm strategies," *Journal of electronic science and technology of china*, vol. 5, no. 3, pp. 283–287, 2007.